Journal of Rock Mechanics and Geotechnical Engineering 15 (2023) 3244–3255

Contents lists available at ScienceDirect

Journal of Rock Mechanics and Geotechnical Engineering

journal homepage: www.jrmge.cn

Full Length Article

Thermal integrity profiling of cast-in-situ piles in sand using fiber-optic distributed temperature sensing

Jing Wang [a,b], Honghu Zhu [a,*], Daoyuan Tan [b], Zili Li [c], Jie Li [a], Chao Wei [a], Bin Shi [a]

[a] *School of Earth Sciences and Engineering, Nanjing University, Nanjing, 210023, China*
[b] *Department of Civil and Environmental Engineering, The Hong Kong Polytechnic University, Hung Hom, Kowloon, Hong Kong, China*
[c] *Department of Civil and Environmental Engineering, School of Engineering and Architecture, University College Cork, College Road, Cork, T12 K8AF, Ireland*

ARTICLE INFO

Article history:
Received 2 November 2022
Received in revised form
5 January 2023
Accepted 16 February 2023
Available online 20 April 2023

Keywords:
Geotechnical monitoring
Distributed temperature sensing (DTS)
Pile defect
Fiber-optic thermal integrity profiling (FO-TIP)
Heat transfer
Pile–soil interface

ABSTRACT

Defects in cast-in-situ piles have an adverse impact on load transfer at the pile–soil interface and pile bearing capacity. In recent years, thermal integrity profiling (TIP) has been developed to measure temperature profiles of cast-in-situ piles, enabling the detection of structural defects or anomalies at the early stage of construction. However, using this integrity testing method to evaluate potential defects in cast-in-situ piles requires a comprehensive understanding of the mechanism of hydration heat transfer from piles to surrounding soils. In this study, small-scale model tests were conducted in laboratory to investigate the performance of TIP in detecting pile integrity. Fiber-optic distributed temperature sensing (DTS) technology was used to monitor detailed temperature variations along model piles in sand. Additionally, sensors were installed in sand to measure water content and matric suction. An interpretation method against available DTS-based thermal profiles was proposed to reveal the potential defective regions. It shows that the temperature difference between normal and defective piles is more obvious in wet sand. In addition, there is a critical zone of water migration in sand due to the water absorption behavior of cement and temperature transfer-induced water migration in the early-age concrete setting. These findings could provide important insight into the improvement of the TIP testing method for field applications.

1. Introduction

Cast-in-situ piles are widely used as deep foundations for superstructures, such as high-rise buildings, bridges, and offshore wind power stations. The soil from the unstable strata in the borehole can be easily brought into the pile as the foreign substance, resulting in defects of different types and sizes (O'Neill et al., 2003; Tabsh et al., 2005; Alipour and Eslami, 2019). These various structural defects can potentially have a negative impact on the bearing capacity of cast-in-situ piles and load transfer at the pile-soil interface, bringing potential risks to the construction and operation of civil infrastructures.

The integrity and quality testing of large and long cast-in-situ piles poses new challenges in foundation construction, requiring advanced methods for detecting voids, honeycombing, necking and other construction quality problems. Various methods have been developed and applied in engineering practice, such as the static load test, sonic pulse-echo (SPE) testing, and cross-hole sonic logging (CSL). However, these conventional methods are generally implemented a month after pile construction and have difficulty in comprehensively evaluating pile parameters (Johnson and Mullins, 2007; ASTM D6760-16, 2016; Hong et al., 2019; Su et al., 2020). In recent years, thermal integrity profiling (TIP) has emerged as a novel and efficient integrity testing method for detecting structural defects of cast-in-situ piles based on the temperature profiles at the early stage of construction (Mullins and Kranc, 2004; Pauly, 2010; Likins and Mullins, 2011; Liu et al., 2020). In engineering practice, the concrete thickness of piles is not always uniform along the depth, which can be reflected by thermal profiles. TIP can sensitively detect structural defects during pile construction and effectively reduce the construction period compared to other methods (Ashlock and Fotouhi, 2014; Johnson, 2014; Boeckmann and Loehr, 2019; Mullins et al., 2021).

* Corresponding author.
E-mail address: zhh@nju.edu.cn (H. Zhu).
Peer review under responsibility of Institute of Rock and Soil Mechanics, Chinese Academy of Sciences.

https://doi.org/10.1016/j.jrmge.2023.02.028

Over the past decade, the relationships between common defects in concrete piles and anomaly of temperature profiles have been investigated (Zhong et al., 2018; Zhong and Deng, 2020; Deng et al., 2021; Sun et al., 2021). Rui et al. (2017) measured the change in concrete curing temperature profiles during the concrete final setting and inferred the thickness of the concrete cover by simulating the heat transfer process between concrete and adjacent ground. Sun et al. (2022) proposed an anomaly detection approach, which combines early-age temperature monitoring data and finite element back-analyses, to be used to reconstruct as-built pile 3D shape and identify anomalous regions inside or outside the pile reinforcement cage. The purpose of their field experiments and simulations is to focus on temperature changes within the borehole. The behavior of cement hydration is affected by many different factors, such as temperature, pressure and water content of the surrounding environments (Reddy et al., 2009). Hence, the behavior of the surrounding soils in the borehole has an equally significant impact on the pile integrity compared to the material properties of the concrete (Liu et al., 2020). The influence of the thermo-hydro-mechanical process in pile concrete and soil on pile defect detection is rather complex. Understanding the transfer of temperature and water around cast-in-situ piles is of importance to ensure the reliability of the TIP method.

Conventionally, temperature monitoring in geotechnical engineering is generally conducted using point thermocouples or array thermometers, which can only provide discrete measurements at specific locations (Mullins, 2010; ASTM D7949-14, 2014). As an alternative, the newly developed fiber optic technology has the advantage of denser measuring points, higher accuracy, ease of installation, and short response time compared with conventional techniques. In addition, field monitoring systems equipped with fiber optic sensors are less susceptible to electromagnetic interference (EMI) and the quality of waterproof measures will not significantly affect the durability (long-term performance) of these sensors as they are made of silicon glass. The fiber optic nerve system (FONS) is capable of measuring continuous and highly detailed strain and temperature profiles of pile foundations and other geotechnical structures during the curing and service periods (Ye et al., 2022; Zhu et al., 2022; Wang et al., 2023; Wu et al., 2023). The distributed strain measurements recorded by the fiber optic sensors can be used to estimate the bearing capacity and reflect the positions and severity of imperfections inside anomaly piles (Lee et al., 2004; Klar et al., 2006; Doherty et al., 2015; Mohamad et al., 2016; Song et al., 2020; Wang et al., 2021; Xu et al., 2021; Zheng et al., 2021; Kou et al., 2022).

This paper investigated the feasibility of the fiber-optic thermal integrity profiling (FO-TIP) method for cast-in-situ piles in sand, with a focus on the transfer of heat and water at the pile-soil interface. A series of model tests was conducted in laboratory, where fiber optic (FO) cables were installed on reinforcement cages and surrounding sand to monitor temperature variations during cement hydration reaction. The study analyzed the relationship between distributed temperature profiles and structural defects, as well as the influence of temperature and water content changes on the detection of pile defects. The findings provide a useful reference for implementing the FO-TIP method of cast-in-situ piles in the field.

2. Experimental procedures of model tests

2.1. Optimization of model dimension and cement mixing ratio

In this study, several model piles were cast in laboratory. According to the experience in previous studies (Fellenius et al., 2009; Liang et al., 2019; Sasaki et al., 2019; Ying et al., 2021), the cement slurry was injected into the hole instead of the concrete due to the limitation of laboratory test size. The water-cement-sand mixing ratio (W:C:S) of 0.44:1:1.83 was selected for pile casting in this study considering its efficient generation of hydration heat (fast and high temperature increase) and good fluidity, similar to the study of Fellenius et al. (2009). The cement grade was using C25, and the sand was the same as that surrounding the model piles. Several model piles were prepared to validate the model dimensions and material parameters. The temperature variation curves during hydration process are plotted in Fig. 1. The temperature increment of the soil at a distance of $3r$ (r is the pile radius) was close to that of the laboratory during testing, which is smaller than expected. It may be due to the relatively small heat generation of the model piles used in this study. Meanwhile, part of the heat is absorbed by the surrounding sand and water, and the pile-soil interface also has a sound thermal resistance. Based on the test results, an optimized model size of $3r$ can ensure that the lateral boundaries exert a negligible influence on temperature transfer in the model tests.

2.2. Model piles

The test setup is shown in Fig. 2. The model piles were 0.15 m in diameter (d) and 0.7 m in length (l). The reinforcement cages of the model piles were prefabricated with an outer diameter of 0.13 m. The reinforcement cage was placed in the center of the test container with 0.6 m in diameter and 0.8 m in length. To investigate the water migration of sand around piles, the drainage valve of the test container was closed and an undrained condition was assumed. The distance between the pile surface and the test container was 0.225 m, which was approximately $3r$. As mentioned previously, the heat of hydration usually has a negligible influence on the soil beyond a distance of $3r$. Therefore, it is reasonable to use the test container to carry out the model tests. In addition, the air temperature in the laboratory was well controlled during the tests to minimize its impact on test results.

According to the method in Fellenius et al. (2009), the model piles were cast by grouting inside a temporary casing (a PVC pipe, see Fig. 3a) with the reinforcement cage placed in the pipe center. Before the cement slurry was injected, the surrounding sand was compacted and filled in layers, and different types of sensors were installed at the same time. In order to prevent hole collapse, the PVC pipe was not taken out at once during cement pouring. First, the PVC pipe was lifted vertically 0.2 m high (Fig. 3b). Then, the remaining cement slurry was gradually injected until the liquid level reached the bottom of the PVC pipe (Fig. 3c). The steps were repeated until the pouring was completed.

Three model tests were conducted on one normal pile and two defective piles with preset defects to investigate the performance of

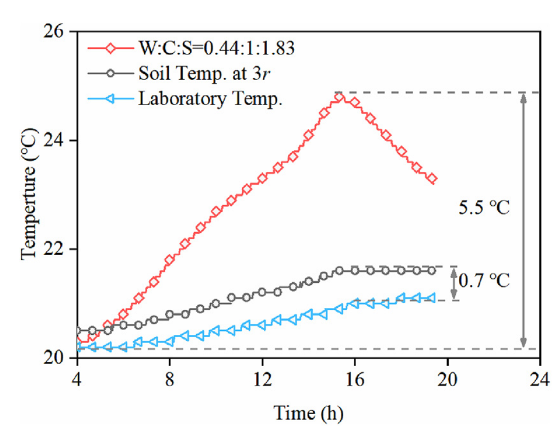

Fig. 1. Temperature variation curves of a model pile during the hydration process. Temp. is short for temperature.

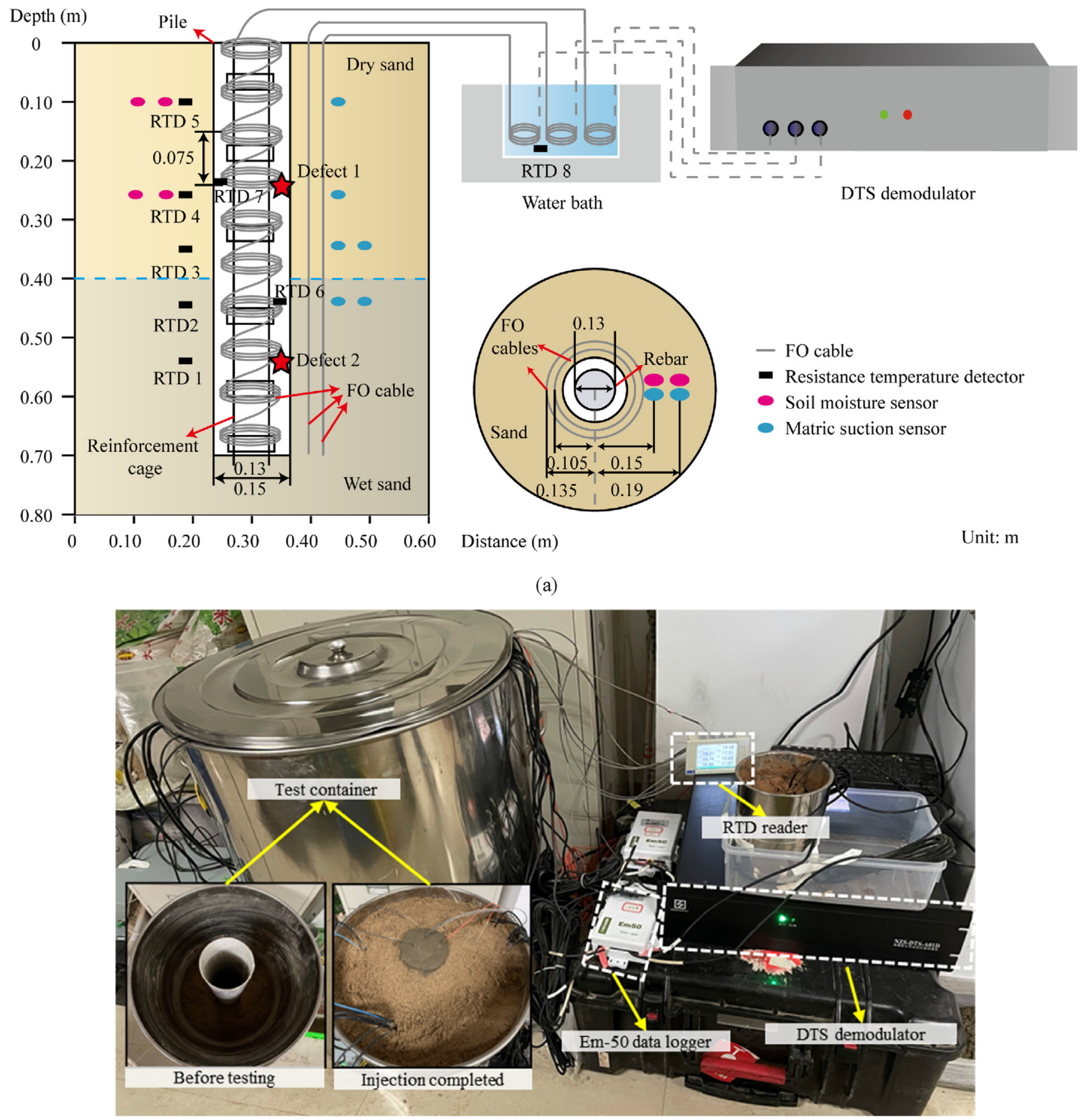

Fig. 2. Laboratory model tests: (a) Schematic diagram of the test setup, and (b) Annotated photographs of apparatus and test setup. RTD and DTS are short for resistance temperature detector and distributed temperature sensing, respectively.

TIP in pile integrity detection. As shown in Fig. 4, the inclusions were a set of sandbags filled with the sand installed externally to the reinforcement cage at two different locations (Boeckmann and Loehr, 2019; Sun et al., 2021). The configuration of pile defects is tabulated in Table 1. Note that the construction disturbance to the surrounding stratum during drilling and the stress disturbance of concrete to the surrounding stratum during injection were not considered in this experiment.

2.3. Test soil

When the permeability of the stratum is lower than 0.1 mD, the cement cannot absorb water from the soil (Sasaki et al., 2018). Therefore, in order to investigate the influence of cast-in-situ piles on the water migration, the sand with permeability greater than 0.1 mD was adopted in this study. The test soil was taken from a construction site in Nanjing, China. As depicted in Fig. 5, the particle size distribution curve was determined by the dry sieving method. The soil was classified as well-graded sand with silt (SW-SM) according to the Unified Soil Classification System (ASTM D2487-17, 2017). The physical properties of the sand were summarized in Table 2. The thermal conductivity of sand with different water contents was measured by actively heated fiber Bragg grating (AH-FBG) (Cao et al., 2018; Wang et al., 2020; Wu et al., 2021; Zhu et al., 2023).

The hydration heat transfer at the pile–soil interface was affected by the water content in the surrounding soil. Special attention should be given to the change in the water content of sand. Therefore, the water contents of sand were set different vertically. The sand was uniformly mixed with water, and the mixture was then filled by layered deposition. After the compaction of every soil layer, the water content of the soil was measured using

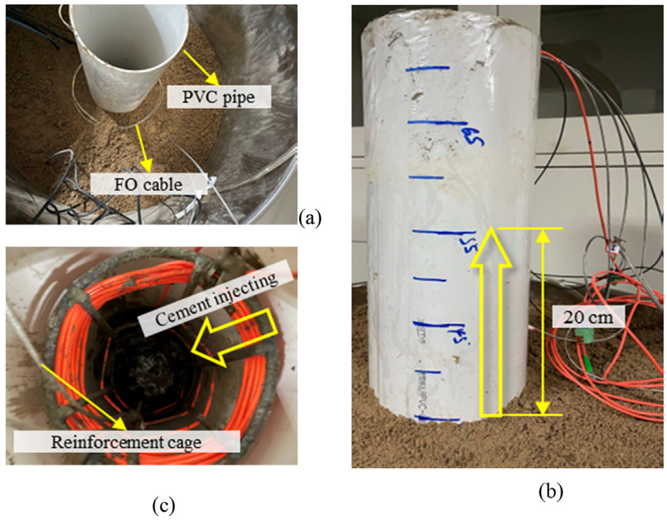

Fig. 3. Casting process of the model piles: (a) Placing the Polyvinyl Chloride (PVC) pipe and filling sand around it in stages; (b) Lifting the PVC pipe; and (c) Injecting the cement slurry.

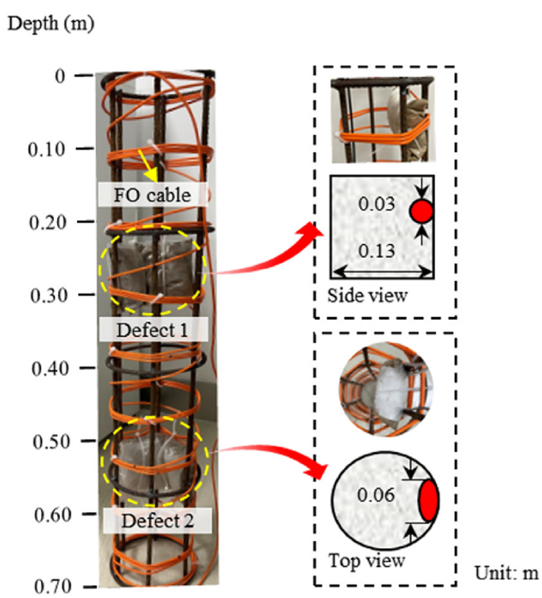

Fig. 4. Layout of pre-set pile defects installed on the reinforcement cage.

Table 1
Configuration of pile defects.

Pile type	Test No.	Depth of the defect (m)	Defect dimension (m)	Mass (kg)
Normal pile	P1	–	–	–
Defective pile	P2, P3	0.18–0.24	0.06 × 0.03 × 0.03	0.2
		0.56–0.61	0.06 × 0.03 × 0.03	0.2

frequency domain reflectometry (FDR) sensors. The initial volumetric water contents θ and degrees of saturation Sr of each soil layer were measured, as listed in Table 3.

2.4. Temperature monitoring using fiber optic sensors

The variations in certain physical quantities, such as strain and temperature, induce lattice oscillations within an optical fiber. The working principle of Raman spectrum distributed temperature sensing (DTS) is the temperature-dependent backscattering of photons at a higher and lower frequency than the original laser pulse. A very small amount of light travels back (backscattered) at each point of the fiber, enabling it to measure any changes along the fiber (Fig. 6). Unlike incident light, this scattered light is called Raman scattering, and its spectral offset is equivalent to the resonant frequency of lattice oscillation. The light scattered back from the optical fiber contains three different spectral shares: Rayleigh scattering, the Stokes component, and the anti-Stokes component. The intensity of the so-called anti-Stokes component is related to temperature, whereas the so-called Stokes component is actually independent of temperature. Based on the Raman optical time domain reflectometry (ROTDR) technology, the local temperature of the optical fiber is derived from the ratio of the anti-Stokes and Stokes light intensities and the time required for the backscattered light to return to the detection unit (Selker et al., 2006; Tyler et al., 2009). Compared with other fiber optic sensing technologies, DTS can measure the temperature distribution along FO cables without the interference of strains.

The hydration reaction of cement slurry results in volume shrinkage and heat generation, which is manifested in the changes

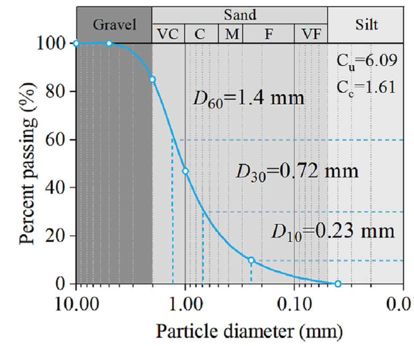

Fig. 5. Particle-size distribution of the soil.

Table 2
Physical properties of the sand.

Depth (m)	Dry density (g/cm)	Thermal conductivity (W/(m K))	Unit weight (kN/m^3)	Saturated permeability coefficient (cm/s)
0–0.3	1.58	1.81	2.68	1.03×10^{-2}
0.3–0.7	1.6	1.91	2.68	1.03×10^{-2}

Table 3
Volumetric water contents (θ) and degrees of saturation (S_r) measured before the tests.

Depth (m)	Test No.	θ (m^3/m^3)	S_r (%)
0.15	Test 1	0.1	24.14
	Test 2	0.09	22.41
	Test 3	0.07	19.32
0.25	Test 1	0.09	21.73
	Test 2	0.07	17.43
	Test 3	0.06	16.9
0.4	Test 1	0.2	49.17
	Test 2	0.1	24.59
	Test 3	0.18	44.26
0.5	Test 1	0.23	56.55
	Test 2	0.3	73.76
	Test 3	0.17	41.8

of strain and temperature. The DTS demodulator used in this study is based on ROTDR to measure temperature distributions, which is basically unaffected by strains. Typically, the DTS systems can locate the temperature to a spatial resolution of 1 m with an accuracy of approximately ±1 °C at a resolution of 0.01 °C. The accuracy of temperature measurements can be calibrated using cold and warm water baths (Gilmore et al., 2019; Lapo et al., 2020). Generally, a FO cable is designed for temperature measurement purposes, which is referred to as a 62.5/125 multimode optical fiber. The sketch of the FO cable is depicted in Fig. 6. In this study, the polyurethane coating was added outside the temperature sensing optical fiber to prevent it from breaking due to the shrinkage of cement slurry. The optical fiber with a polyurethane coating was still able to monitor rapid thermal responses in the surrounding environment.

The installation layout of the FO cables is illustrated in Fig. 2a. Cables were wrapped into one helix held together with the reinforcement cage (see Fig. 4). To increase the resolution of the DTS system, FO cables were wound into three circles at the same depth. The temperature data of the cables in the middle circles were least affected by the temperature of other locations. Therefore, they were taken as the true values of temperature in the following investigations. The interval of each spiral along the depth direction was 0.075 m. The FO cables, which were wound into two spirals and buried in the soil, were also installed to study the thermal diffusion between the pile and surrounding strata. The helixes had internal radii of 0.105 m and 0.135 m, respectively. The start and end of the FO cables passed through the water bath in this study for temperature calibration. One PT100 RTD with measuring accuracy ±0.1 °C was placed in the water bath to record calibration temperatures. The other seven RTDs were installed in the pile and soil for temperature calibration of fiber optic measurements. The NZS-DMS-A01 DTS demodulator has a spatial resolution of 1 m and a sampling interval of 0.05 m. After the cement slurry was injected, the DTS demodulator began collecting the data with a sampling interval of 5 min.

2.5. Monitoring of soil water contents and matric suctions

The relative locations of the water content sensors and matric suction sensors are shown in Fig. 7. A total of six soil moisture sensors and four matric suction sensors were installed across the height and radial direction of the test container. Specifically, four rows of EC-5 soil moisture sensors produced by METER Group company were buried in the sand at depths of 0.1 m, 0.15 m, 0.35 m, and 0.45 m from the ground surface, respectively. In the horizontal direction, four soil moisture sensors were embedded at distances of 0.15 m and 0.19 m from the pile center and their depths were 0.35 m and 0.45 m, respectively. There was only one sensor at 0.1-m or 0.15-m depths. These sensors were individually calibrated with material-specific calibration curves with an ultimate accuracy of ±0.06 m^3/m^3. The matric suction sensors were from Decagon Devices Inc., Pullman, USA (METER Group, 2017), known as TEROS 21, with the working principle of using two fixed-matric porous ceramic discs (dielectrics) separated by a printed electric circuit board to form a capacitor. They can measure matric suctions up to 100 kPa with a resolution of ±0.05 kPa. The accuracy of these sensors is highly influenced by the states of preexisting and entered air bubbles. Full saturation in the model preparation was applied to minimizing the time delay in the response of the matric suction sensors. At the depths of 0.1 m and 0.25 m in the sand layers, the matric suction sensors were buried 0.15 m and 0.19 m away from the pile center (horizontal direction). Em-50 data loggers were used to collect the data of soil water contents and matric suctions.

The properties of cement slurry mainly change at the early stage of the hydration reaction of cement. The contribution from thermal

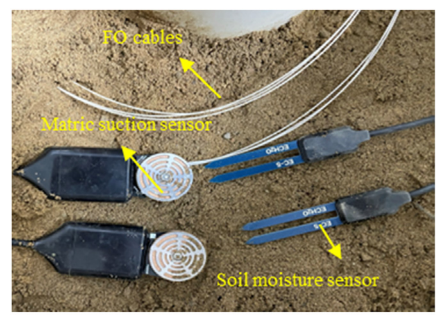

(a)

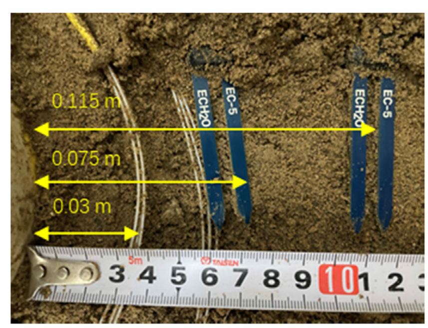

(b)

Fig. 7. Photographs of sensors (a) Soil moisture sensors (EC-5) and matric suction sensors (TEROS 21), and (b) Relative locations of sensors.

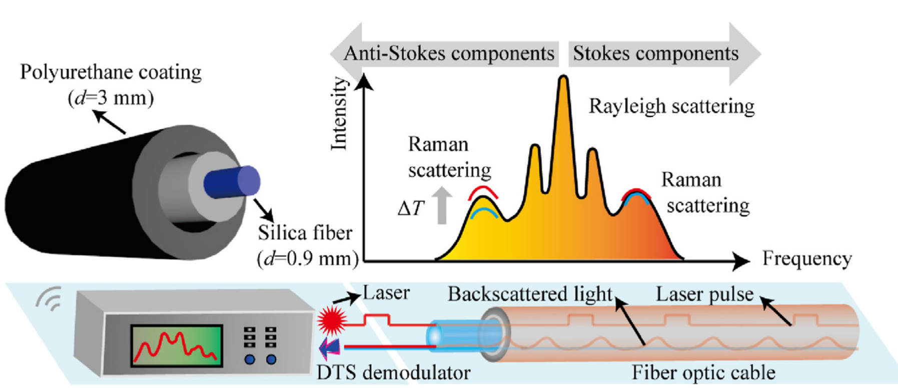

Fig. 6. Principle of the DTS technique and sketch of the FO cable. ΔT is the temperature variation.

strain is pronounced during the first 5 h of shrinkage since the initial set and becomes negligible after 24 h (Zhen and Xiong, 2013). Therefore, pile and soil temperatures, soil water contents and matric suctions in the tests were continuously measured for about 24 h. In addition, if the cement slurry is surrounded by the sand with high permeability, the volume shrinkage will not be significant since the cement can absorb sufficient water from the surrounding sand to compensate for its hydration process. Therefore, the volume shrinkage of the cement slurry was not measured in this study.

3. Results

3.1. Heat transfer of cast-in-situ piles and sand

For the normal pile P1 and defective pile P3, spatiotemporal distributions of temperature are illustrated in Fig. 8. There was an obvious "attenuation" at both ends of the longitudinal temperature profiles. The peak temperatures of the pile head and toe were 22 °C and 23 °C, respectively, which were both lower than the peak temperature in the middle of the piles (25 °C), as shown in Fig. 8a. The attenuation depth ranges of the pile head and toe were 0–0.15 m and 0.6–0.7 m, respectively. The heat of the piles was not only radially dissipated outward the soil but also vertically dissipated to the air at the top and to the soil at the bottom. The spatiotemporal distributions of temperature along the piles shaped a different "spindle", which were in good agreement with the findings by Johnson (2014) and Sun et al. (2021). The abnormalities in the temperature profiles of the defective pile P3 gradually became obvious before reaching the peak temperature, particularly at side B closer to the preset defects. The temperatures near depths of 0.2 m and 0.50 m were obviously lower than that at other depths, which matched the locations of the defects. The time for the abnormal temperature of the defective pile P3, which can be called the time window for detecting defects, was approximately 13 h (the peak temperature stage) and 20 h (the cooling stage). It indicates that the location of defects can be preliminarily determined from the time history curves of the pile temperatures.

Fig. 9 shows the spatiotemporal distributions of temperatures in the sand at different distances away from the center of the normal pile P1 and defective pile P3. The abnormal location of the temperature in sand was consistent with that in the defective pile P3, both at depths of 0.2 m and 0.5 m. However, the temperature difference in sand was less than that of pile P3, which was 2 °C approximately. The heating period of the defective pile P3 lasted approximately 7.5 h, which was 75% of the duration of the overall pile heating period (10 h). The time to reach the peak temperature in sand was approximately 0.5 h later than that in the pile, which was due to the hysteresis of temperature transfer. The temperature difference in sand at the cooling stage was very small. From the temperature profiles of sand around the normal pile P1, it displayed that there was only a one time-window for the detection of pile defects. The reasonable selection of a time window is critical to the detection accuracy of pile defects using the FO-TIP method.

According to the temperature distribution in the piles and sand (Figs. 8 and 9), the peak temperature of the defective pile P3 center at 0.2 m depth (defect 1) was obviously lower than that of the normal pile P1. The peak temperature of the defective pile P3 center at 0.3 m depth (without defects) was close to that of the normal pile P1. This shows that the existence of defects had little effect on the hydration heat at the normal location near the defects. However, the temperatures in the soil at the defect positions were lower than that without defects. In other words, the existence of pile defects may not significantly affect the heat transfer of other positions of

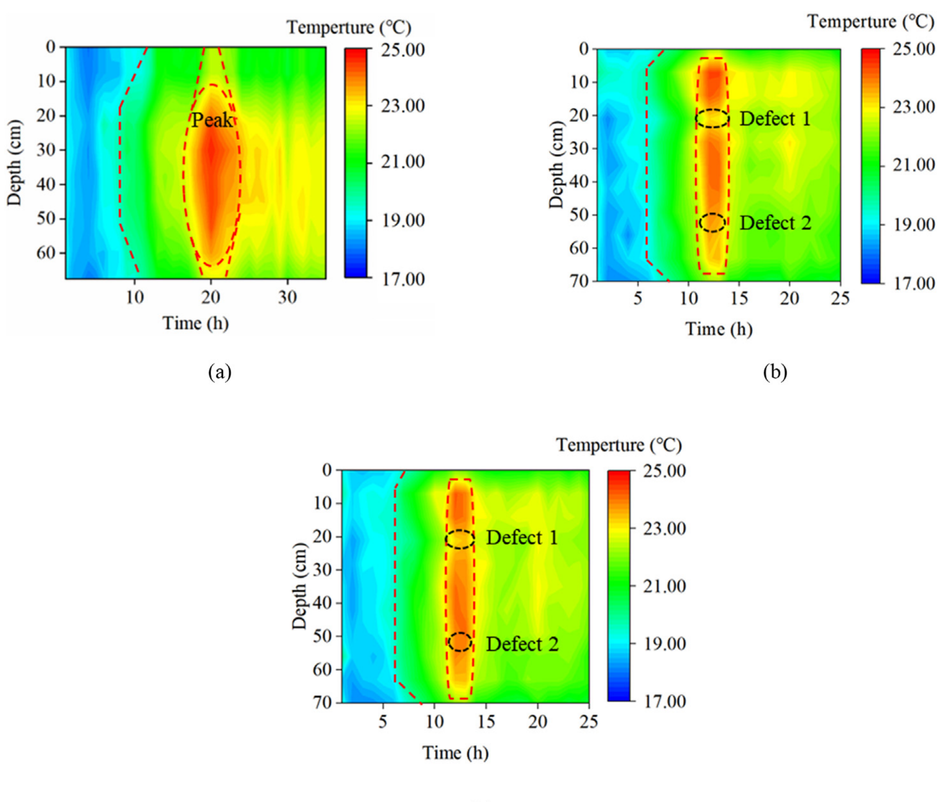

Fig. 8. Spatiotemporal distributions of temperature in the pile shafts: (a) The normal pile P1, (b) Side A of the defective pile P3, and (c) Side B of the defective pile P3.

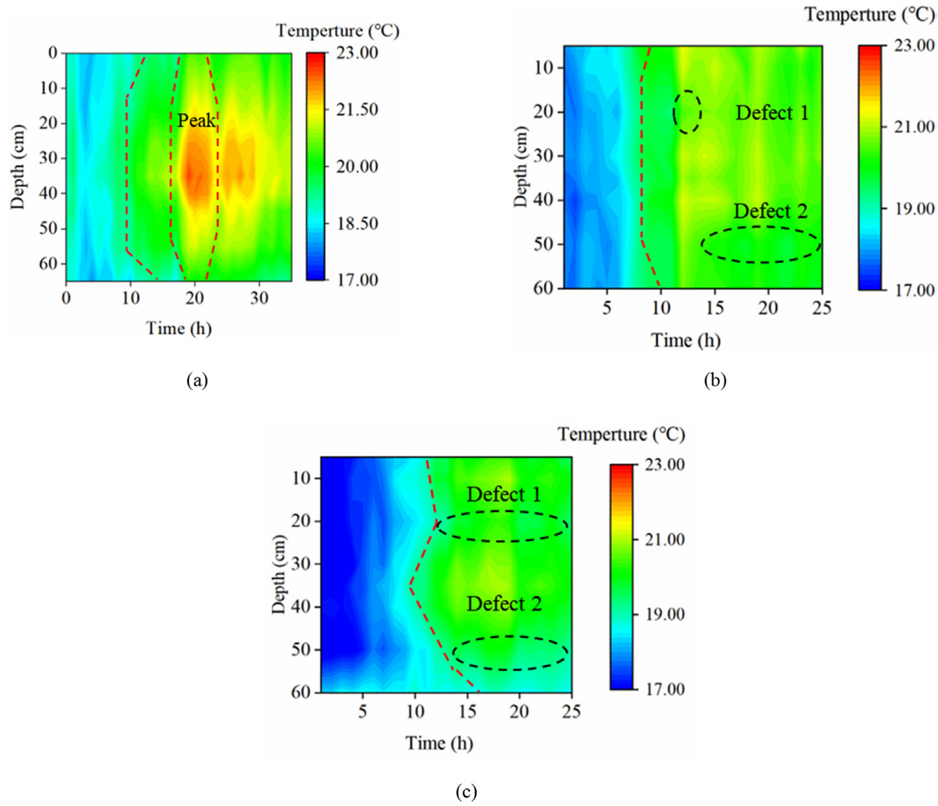

Fig. 9. Spatiotemporal distributions of temperature in sand (a) 10.5 cm away from the center of the normal pile P1; (b) 10.5 cm away from the center of the defective pile P3; and (c) 13.5 cm away from the center of the defective pile P3.

the pile but can affect the heat transferred to the surrounding soil. During the hydration reaction, the water contents of sand layers around the pile varied at different depths, which in turn influenced directly the degree of hydration reaction in the piles. The hydration reaction process of piles can be accelerated with increase of the degree of saturation of soil around the pile. This scenario in the defective pile was not evident. The water absorption of cement at some locations was reduced due to the existence of defects, while more water can be used for cement hydration reaction at other locations. The low water content of the soil at the same depth with the defects pile led to a low efficiency of the hydration reaction of piles. Therefore, the soil temperature at the defect's positions was lower than that at the other positions.

The temperature profile of the normal pile had a large roll off at the pile toe. The abnormally low values were not entirely due to end effects. After excavation, it was found that the pile surface was intact (Fig. 10a) but the sufficient thickness of sediment at the pile toe and the cement sand slurry did not completely wrap the reinforcement cage (Fig. 10b). The soft toe conditions of the normal pile, which were similar to the "soft base" caused by inadequate cleaning of the base of model piles, were an accident. During the pile casting, the reinforcement cage slowly extended into the sand at the bottom. Therefore, the cement mortar could not completely cover the bottom of the reinforcement cage. In the following construction of other piles, the reinforcement cage was well fixed, so there was no abnormality at the pile toes. It should be pointed out that the outer surface of the pile at the defective part of the prefabrication was flat. However, mud inclusions and holes appeared in the pile surface far away from defects, as shown in Fig. 10c and d. The hole collapsed during the hydration reaction. Due to the low water content of the surrounding soil, sand and cement slurry could not be well mixed together.

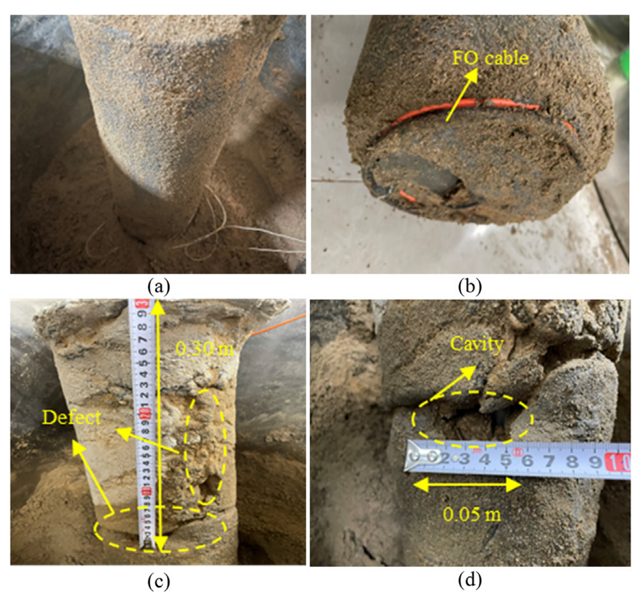

Fig. 10. Photographs of pile shafts: (a) Integrated surface of the normal pile, (b) Bottom of the normal pile, (c) Surface of the defective pile, and (d) Size of the defects on the pile surface.

3.2. Structural defect evaluation

The location of defects can be roughly identified from the temperature profiles, but the size of defects can hardly be estimated. Fig. 11 shows the measured temperature curves of normal

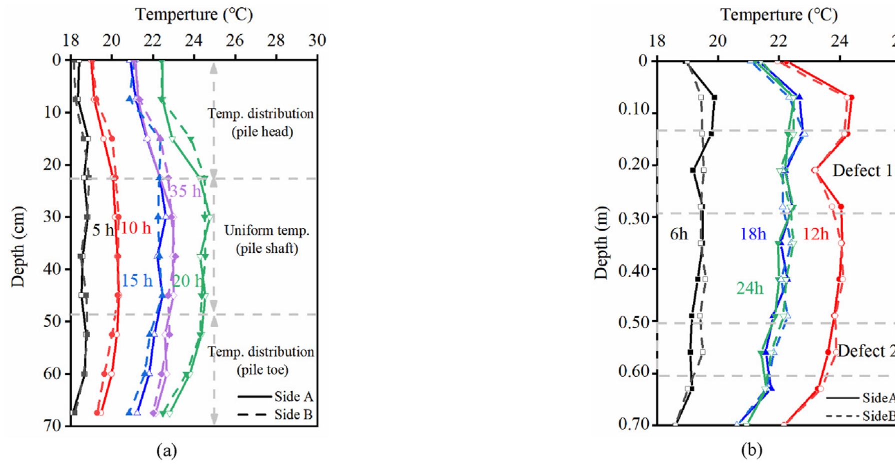

Fig. 11. Temperature curves of pile shafts at different ages: (a) The normal pile P1, and (b) The defective pile P3.

and defective piles along the pile shafts. According to the temperature distribution of the piles, the total length was mainly divided into three zones, including the temperature diffusion zone at the pile head, the temperature distribution zone in the middle of the pile, and the temperature diffusion zone at the pile toe. Defects can be identified by analyzing the temperature profiles measured along the piles. The diameter of the corresponding preset defects at 0.2 m and 0.5 m was 20% of the pile diameter, and the peak temperatures were approximately 1.3 °C and 0.5 °C lower than the temperature at other locations, respectively. The temperature reduction rate was lower than the expected defect ratio due to the heat transfer in different media. Because there are many factors affecting the hydration heat production of cement, the calculation is prone to errors in practical engineering. It should be noted that this method is only applicable to estimating the relative size of the pile diameter compared with different positions along the depth direction.

During the tests, the FO cables embedded in the piles can acquire the temperatures in real time. The FO-TIP method can provide a continuous vertical temperature distribution and discrete transverse temperature measurement. The vertical temperature profile can detect and locate any bulges, necks, or inclusions that exist in the depth direction (axial direction). However, the FO cables can only be installed on reinforcement cages of piles (axial direction) and therefore cannot completely cover the entire radial area. In other words, the temperature information of the radial area is limited. In addition, the measured temperature value would deviate from the theoretical value due to the loss of heat transfer between the surrounding stratum and the pile. Thus, there is a need to improve the analysis methods to indicate transverse defect characteristics.

It is assumed that the internal temperature distribution of the normal piles is roughly bell-shaped, and the peak temperature apparently appears in the core of piles and decreases radially toward the surrounding soil, as shown in Fig. 12 (Johnson, 2014; Sun et al., 2021). In soil and rock, the heat transfer is mainly conductive. There is a unique temperature curve available according to the

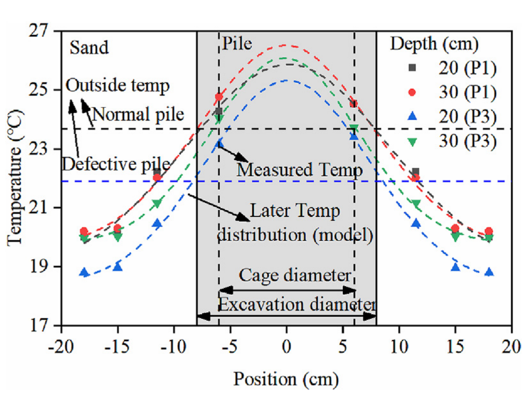

Fig. 12. Modeled temperature distributions across a diameter shaft at a given depth.

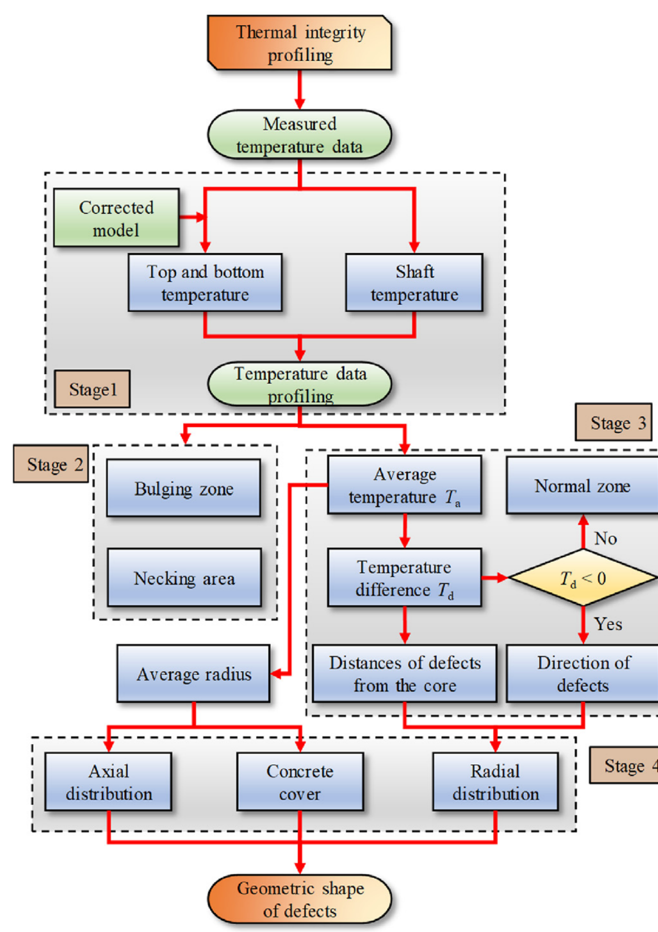

Fig. 13. Evaluation system for pile defects.

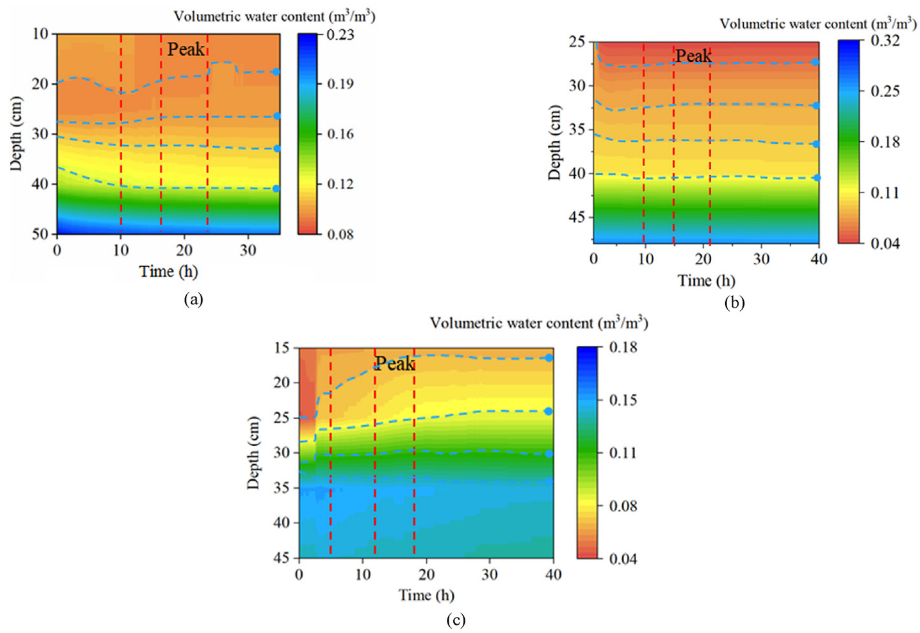

Fig. 14. Spatiotemporal distributions of water contents in the sand at 15 cm away from the pile centers: (a) P1, (b) P2, and (c) P3.

mixture design and site conditions. The total amount of heat generated by each material depends on its weight fraction P relative to the total cementitious materials (Kim et al., 2003; Schindler and Folliard, 2005; Mullins, 2010; He et al., 2020). Although the temperature changes with time, the characteristics of the profile do not change. Heat calculations can be converted to interpretation to identify the radial location of imperfections. The specific steps are based on the following assumptions:

(1) The concrete in the pile is assumed to be uniformly mixed, and the heat generation and heat transfer of the concrete in the same radial position are the same.
(2) The properties of mud inclusion defects at the same location are assumed to be consistent.
(3) The influence of the surrounding soil on heat transfer is not considered temporarily.

The FO-TIP based pile performance evaluation method provides a powerful tool for the quality inspection of piles, as shown in Fig. 13. In engineering practice, the temperature profiles measured by FO cables and the radial temperature distribution fitted by the model can accurately characterize the information of defects at different positions of piles in multiple directions and three dimensions. The TIP method using DTS technology will not only effectively detect structural defects of piles, but also may be helpful in enhancing understanding of the behavior of piles. Early identification of pile defects can greatly improve the efficiency of civil

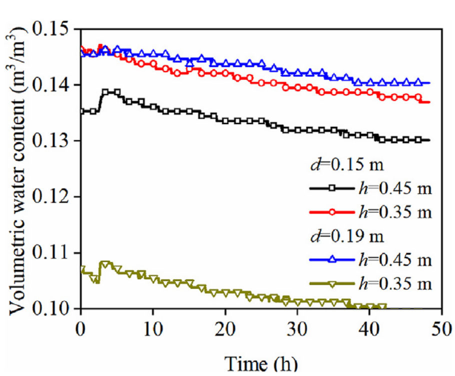

Fig. 15. Variations of water contents in the sand at 0.15 m and 0.19 m away from the center of the defective pile P3.

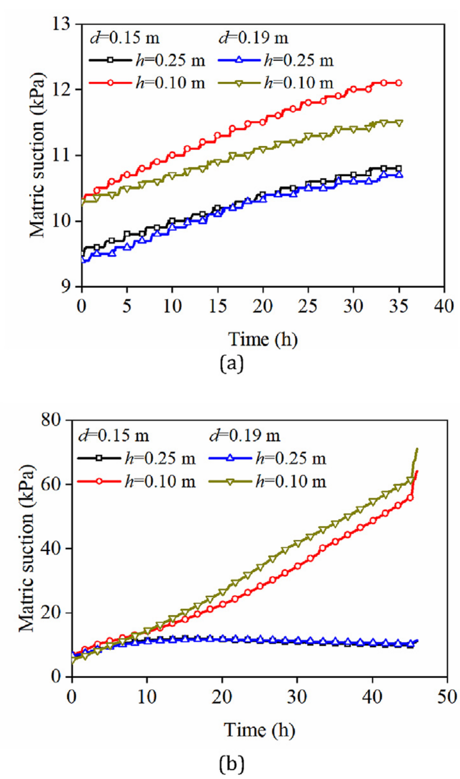

Fig. 16. Variations of matric suction in the sand at 0.15 m, and 0.19 m away from the pile centers: (a) P1 and (b) P3.

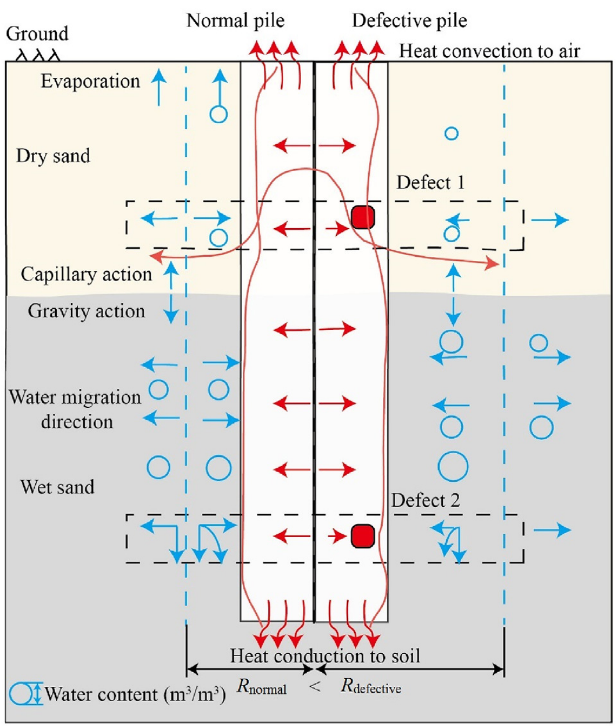

Fig. 17. Schematic diagram of hydro-thermal change of normal and defective piles. R_{normal} is the critical radius $R_{critical}$ of the normal pile, and $R_{defective}$ is the critical radius $R_{critical}$ of the defective pile.

infrastructure construction and enable intelligent monitoring throughout the life cycle.

The information of defects in the radial direction can be interpreted according to the steps of stage 3, as shown in Fig. 13. The first step involves calculating the average radius of the shaft by taking the average of the total volume and length of the shaft, and obtaining the average temperature T_a of the entire shaft by averaging the TIP data over its entire length. The next step is to calculate the temperature difference T_d between the measured peak temperature and the average temperature at different angles at a particular depth, where a negative T_d indicates the location of a defect. In the third step, the size of the defect in the radial direction can be determined for each depth based on the previous calculation, and the distance from the defect to the core can be estimated. Different positions of defects from the core can result in varying levels of heat transfer loss in the core, which in turn reduces the measured temperature value. The relationship between the distance (d_d) between the defect and the core and the temperature reduction T_d of the measuring points can be established by combining the measured data and FEM analysis. The temperature anomaly T_d is brought into the relationship to obtain the distance between the defect and the pile core. The key point to determine the radial information of pile defects is to determine the relationship between d_d and T_d. The temperature profile is affected by the type and size of the defect. It is not reliable to determine the size of defects only by the temperature profile in this paper. To identify the material type of the defect, physical property profiles of different positions in the pile are needed.

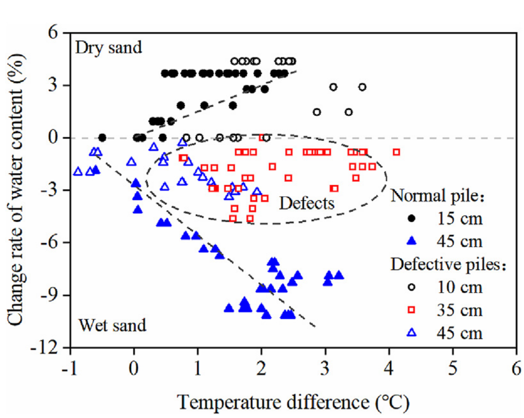

Fig. 18. Temperature difference between the pile and soil and change rate of water content at different depths of normal and defective piles.

3.3. Development of water content of the surrounding soil

Defects of the piles also arise from the properties of the localized soils around the borehole becoming softer or weaker. It is necessary to investigate comprehensively the mechanism and influencing factors of hydration heat transfer from bored piles to surrounding soils to help locate and evaluate defects in piles. The change in the water content of sand with different radii versus time is shown in Figs. 14 and 15. During the rising period of hydration heat, the water content of dry sand around the pile decreased by approximately 0.05 m^3/m^3, while the water content of wet sand generally increased by approximately 0.1 m^3/m^3. The change in water content mainly occurred at the heating stage of piles, while the peak temperature of sand decreased with increasing water content. The change in water content at the defect location was much lower than that at other locations. The water absorption of cement at some locations was reduced due to the presence of defects, while more water can be used for cement hydration reactions at other locations. The existence of defects not only affects the integrity of the pile but also affects the hydration heat transfer from piles to surrounding soils. The migration of water in the wet sand is only affected by the temperature diffusion and gravity, and the migration of water in the dry sand is also affected by the capillarity. The pressure difference across the cement-formation interface caused outflux of cement pore water, resulting in negative values of absorbed water volume at the beginning of Test 3.

3.4. Development of matric suction of the surrounding soil

The cement volume shrinkage can cause depression of the capillary suction pressure in the wellbore condition where the cement is surrounded by a water-unsaturated formation. The migration of water within the dry sand is also affected by the pore pressure in cement slurry and capillary action. The changes in matric suction in the sand at radii of 0.15 m and 0.19 m were measured, as shown in Fig. 16. The matric suction of the sand varied slightly due to the short test time period. The matric suction at a depth of 0.1 m was higher than that at a depth of 0.25 m. The matric suction at a radius of 0.15 m was also higher than that at a radius of 0.19 m. With decrease in the water content during the hydration process, the suction pressure was generated with decrease in the pore pressure. The more limited the ground water supply, the greater the matric suction. However, with the progress of the hydration process, the pore pressure would return to a stable state over elapsed time, and the increased rate of matric suction slowed down. The matric suction of sand around the normal pile was lower than that measured around the defective pile. The reason may be that bubbles were formed in the cement pores in the defective pile, which reduced the pore pressure and led to an increase in matric suction.

4. Discussion

The permeability of the sand exceeded 0.1 mD in this study, and the provision of sufficient water to the cement was guaranteed. Therefore, water provision to the cement would not be limited at the initial hardening stage. Fluid flow across the contact interface was allowed, enabling the pore water to flow between the sand and cement. Because the pore water in the cement is greater than that of the formation, the water flows from the cement to the sand initially. The piles started to absorb water from the formation due to the hydration. This caused the pore water in sand within a certain radius to migrate to the pile core. As the temperature difference between the pile and soil increased, the water content of the dry sand at a depth of 15 cm of the pile surface increased, while that of the wet sand was just the opposite. The increase range of water content of the wet sand around the defective pile decreased. The results show that the influence of the water content in the sand on the water absorption of the hydration reaction is important. Meanwhile, a large amount of heat was released from the cement and diffused into the sand, forming a temperature gradient. The maximum temperature gradient was 3.5 °C, reaching 70% of the peak temperature. The pore water in the sand was driven by the temperature difference to flow towards positions with lower temperature (away from the pile core), resulting in the redistribution of the water field in the soil. The competing water movement causes complex absorbed water changes at the pile–soil interface.

As shown in Figs. 14 and 15, at a radius of 0.15 m away from the piles, the water content of the sand at a depth of 0.35 m was higher than that at a depth of 0.45 m, but at a radius of 0.19 m away from the piles, an opposite trend was observed. This indicates that the two effects on the pore water reached the equilibrium at a certain radius ($R_{critical}$) from the pile. A schematic diagram of a certain radius $R_{critical}$ from the piles can be seen in Fig. 17. The water in the sand within radius $R_{critical}$ mainly moved to the pile core. Beyond the radius $R_{critical}$, the pore water in the sand would move away from the pile. The position of the critical radius $R_{critical}$ changes with the progress of the hydration reaction. When the water absorption of cement is small, the position of the critical radius $R_{critical}$ coincides with the outside of the pile.

The relationship of the temperature difference between the pile and soil and the change rate of the water content at different depths of the normal and defective piles can be seen in Fig. 18. The temperature gradient at the defect location of the pile was smaller than that at the normal location. The influence of the temperature driving force on the water transfer became smaller. On the other hand, the reduction of the chemical water absorption capacity of the pile at the defect location also led to a small change in water content of the sand. Therefore, defective piles exhibited a lower rate of water content change compared to normal piles when the temperature difference between the soils surrounding piles was the same. The temperature difference between the normal and defective piles is more prominent in the wet sand. The temperature profiles in the TIP method are correlated with water content profiles of the surrounding soil. Meanwhile, the measurement of the physical properties of the pile will be affected by the hydration heat transfer from bored piles to surrounding soils. Due to the size effect, the hydration heat of the pile in model test is far less than that in field tests. The relationship between the hydration heat transfer and pile defects is qualitatively analyzed in this paper. In the future, calibration tests, numerical simulations, and field instrumentation will be carried out to obtain more useful guidelines for the quantitative detection of pile defects.

5. Conclusions

This paper investigates the performance of TIP in integrity detection and performance evaluation of cast-in-situ piles. The model piles were instrumented with fiber optic DTS cables and the temperature variations during cement hydration heat release. The main conclusions are drawn as follows:

(1) The FO-TIP method is capable of identifying necking and inclusion defects by analyzing the temperature profiles. The location of defects can be preliminarily determined from the time history curves of the pile temperature. Selecting an appropriate time window is crucial to detect accurately the pile defects using the FO-TIP method based on temperature data.
(2) The temperature data of FO cables provide a continuous vertical temperature distribution and discrete transverse measurement. Defects can be identified according to the measured temperature profiles of piles, which is applicable only for estimating the pile diameter at different positions along the depth direction. The radial distribution of defects at different positions of piles can be obtained from combining the axial temperatures measured by the FO cables with the radial temperature distribution.
(3) Moisture migration at the pile-soil interface is complex due to the hydration reaction and temperature gradients. The two effects on the pore water reached equilibrium at a certain radius away from the pile. The position of the critical radius changes with progress of the hydration reaction.
(4) The temperature profiles in the TIP method are related to the water content profiles of surrounding soil. The temperature difference between the normal and defective piles is more obvious in wet sand.

Declaration of competing interest

The authors declare that they have no known competing financial interests or personal relationships that could have appeared to influence the work reported in this paper.

Acknowledgments

The authors gratefully acknowledge the financial support provided by the National Natural Science Foundation of China (Grant Nos. 42225702 and 42077235) and the Open Research Project Program of the State Key Laboratory of Internet of Things for Smart City (University of Macau), China (Grant No. SKLIoTSC(UM)-2021-2023/ORP/GA10/2022).

References

Alipour, A., Eslami, A., 2019. Design adaptations in a large and deep urban excavation: case study. J. Rock Mech. Geotech. Eng. 11 (2), 389–399.
Ashlock, J.C., Fotouhi, M.K., 2014. Thermal integrity profiling and crosshole sonic logging of drilled shafts with artificial defects. In: Proceedings of Geo-Congress 2014 Technical Papers, GSP, 234. ASCE, Atlanta, GA, USA, pp. 1795–1805.
ASTM D7949-14, 2014. Standard Test Methods for Thermal Integrity Profiling of Concrete Deep Foundations. ASTM International, West Conshohocken, PA, USA.
ASTM D6760-16, 2016. Standard Test Method for Integrity Testing of Concrete Deep Foundations by Ultrasonic Crosshole Testing. ASTM International, West Conshohocken, PA, USA.
ASTM D2487-17, 2017. Standard Practice for Classification of Soils for Engineering Purposes (Unified Soil Classification System). ASTM International, West Conshohocken, PA, USA.
Boeckmann, A.Z., Loehr, J.E., 2019. Valuation of thermal integrity profiling and crosshole sonic logging for drilled shafts with concrete defects. Transport. Res. Rec. 2673 (8), 86–98.

Cao, D.F., Shi, B., Zhu, H.H., Inyang, H.I., Wei, G.Q., Duan, C.Z., 2018. A soil moisture estimation method using actively heated fiber Bragg grating sensors. Eng. Geol. 242, 142–149.

Deng, W., Zhong, R., Ma, H., 2021. Fiber optic-based thermal integrity profiling of drilled shaft: inverse modeling for spiral fiber deployment strategy. Mater 14 (18), 5377.

Doherty, P., Igoe, D., Murphy, G., Gavin, K., Preston, J., Mcavoy, C., Byrne, B.W., Mcadam, R., Burd, H.J., Houlsby, G.T., 2015. Field validation of fibre Bragg grating sensors for measuring strain on driven steel piles. Géotech. Lett. 5 (2), 74–79.

Fellenius, B.H., Kim, S.-R., Chung, S.-G., 2009. Long-Term monitoring of strain in instrumented piles. J. Geotech. Geoenviron. Eng. 135 (11), 1583–1595.

Gilmore, T.E., Johnson, M., Korus, J., Mittelstet, A., Briggs, M.A., Zlotnik, V., Corcoran, S., 2019. Streambed flux measurement informed by distributed temperature sensing leads to a significantly different characterization of groundwater discharge. Water 11, 2312.

He, X., Chen, Y., Tan, X., Wang, S., Liu, L., 2020. Determining the water content and void ratio of cement-treated dredged soil from the hydration degree of cement. Eng. Geol. 279, 105892.

Hong, W.T., Shin, S.Y., Park, M.C., Lee, J.S., Song, M.J., 2019. Load transfer curve analyses of drilled shafts using crosshole sonic logging test. J. Geotech. Geoenviron. Eng. 145 (7), 04019026.

Johnson, K.R., Mullins, A.G., 2007. Concrete temperature reduction via voiding drilled shafts. Contemporary Issues in Deep Foundations. In: Proceedings of Geo-Denver 2007, GSP, 158. ASCE, Atlanta, USA, pp. 1–12.

Johnson, K.R., 2014. Temperature prediction modeling and thermal integrity profiling of drilled shafts. In: Proceedings of Geo-Congress 2014 Technical Papers, GSP 234. ASCE, Atlanta, USA, pp. 1781–1794.

Kim, K.H., Jeon, S.E., Kim, J.K., Yang, S.C., 2003. An experimental study on thermal conductivity of concrete. Cement Concr. Res. 33 (3), 363–371.

Klar, A., Bennett, P.J., Soga, K., Mair, R.J., Tester, P., Fernie, R., St John, H.D., Torp-Peterson, G., 2006. Distributed strain measurement for pile foundations. Proc. Geotech. Eng., ICE 159 (3), 135–144.

Kou, H., Jing, H., Zhou, N., Chen, Q., Li, W., 2022. Feasibility of bare fiber Bragg grating sensing technology in the measurement of inner wall axial stress along open-ended pipe pile in sand. Struct. Control Health Monit. 29 (4), e2920.

Lapo, K., Freundorfer, A., Pfister, L., Schneider, J., Selker, J., Thomas, C., 2020. Distributed observations of wind direction using microstructures attached to actively heated fiber-optic cables. Atmos. Meas. Tech. 13, 1563–1573.

Lee, W., Lee, W.J., Lee, S.B., Salgado, R., 2004. Measurement of pile load transfer using the fiber Bragg grating sensor system. Can. Geotech. J. 41 (6), 1222–1232.

Liang, X., He, H., Zhang, Y., 2019. Optimization design of micro-piles in landslide safety protection based on machine learning. Saf. Sci. 118, 861–867.

Likins, G., Mullins, G., 2011. Structural integrity of drilled shaft foundations by thermal measurements. Struct. Eng. 46–48.

Liu, Y.L., Ding, H., Wang, K.B., Xiao, H.L., Li, L.H., 2020. Thermal conduction characteristics of DTS when detecting the integrity of cast-in-place piles considering their environment. Heat Mass Tran. 56 (7), 2185–2202.

Mohamad, H., Tee, B.P., Ang, K.A., Chong, M.F., 2016. Characterizing anomalies in distributed strain measurements of cast-in-situ bored piles. Jurnal Teknologi 78 (8), 75–82.

Mullins, A.G., Kranc, S.C., 2004. Method for testing the integrity of concrete shafts. US Patent 6 (783), 273.

Mullins, A.G., 2010. Thermal integrity profiling of drilled shafts. DFI Journal 4 (2), 54–64.

Mullins, G., Johnson, K.R., Winters, D., Hilferding, H., Kupselaitis, K., 2021. Selection of thermal integrity data regression parameters. Geotech. Test J. 44 (3), 741–755.

O'Neill, M.W., Tabsh, S.W., Sarhan, H.A., 2003. Response of drilled shafts with minor flaws to axial and lateral loads. Eng. Struct. 25 (1), 47–56.

Pauly, N., 2010. Thermal Conductivity of Soils from the Analysis of Boring Logs. Master's Thesis. University of South Florida, Tampa, FL, USA.

Reddy, B.R., Xu, Y., Ravi, K., Gray, D., Pattillo, P.D., 2009. Cement-shrinkage measurement in oilwell cementing-A comparative study of laboratory methods and procedures. SPE Drill. Complet. 24 (1), 104–114.

Rui, Y., Kechavarzi, C., O'Leary, F., Barker, C., Nicholson, D., Soga, K., 2017. Integrity testing of pile cover using distributed fibre optic sensing. Sensors 17, 2949.

Sasaki, T., Soga, K., Elshafie, M., 2018. Simulation of wellbore construction in offshore unconsolidated methane hydrate-bearing formation. J. Petrol. Sci. Eng. 60, 312–326.

Sasaki, T., Park, J., Soga, K., Momoki, T., Kawaguchi, K., Muramatsu, H., Imasato, Y., Balagopal, A., Fontenot, J., Hall, T., 2019. Distributed fibre optic strain sensing of an axially deformed well model in the laboratory. J. Nat. Gas Sci. Eng. 72, 103028.

Schindler, A., Folliard, K., 2005. Heat of hydrations models for cementitious materials. ACI Mater. J. 102 (1), 24–33.

Selker, J.S., Thévenaz, L., Huwald, H., Mallet, A., Luxemburg, W., Giesen, N.V.D., Stejskal, M., Zeman, J., Westhoff, M., Parlange, M.B., 2006. Distributed fiber-optic temperature sensing for hydrologic systems. Water Resour. Res. 42, 1–8.

Song, H.B., Pei, H.F., Xu, D.S., Cui, C.Y., 2020. Performance study of energy piles in different climatic conditions by using multi-sensor technologies. Measurement 162, 107875.

Su, M., Zhao, Y., Li, S., Xue, Y., Qiu, D., Wang, P., Kong, F., Xia, T., 2020. Parameter preferences for length detection of reinforcement cage in bored pile. J. Perform. Constr. Facil. 32 (2), 04020002.

Sun, Q., Elshafie, M., Barker, C., Fisher, A., Schooling, J., Rui, Y., 2021. Thermal integrity testing of cast in situ piles: an alternative interpretation approach. Struct. Health Monit. 20 (5), 2493–2512.

Sun, Q., Elshafie, M.Z.E.B., Barker, C., Fisher, A., Schooling, J., Rui, Y., 2022. Integrity monitoring of cast in-situ piles using thermal approach: a field case study. Eng. Struct. 272, 114586.

Tabsh, S.W., O'Neill, M.W., Nam, M.S., 2005. Shear strength of drilled shafts with minor flaws. Eng. Struct. 27 (5), 736–748.

Tyler, S.W., Selker, J.S., Hausner, M.B., Hatch, C.E., Torgersen, T., Thodal, C.E., Schladow, S.G., 2009. Environmental temperature sensing using Raman spectra DTS fiber-optic methods. Water Resour. Res. 45, W00D23.

Wang, M., Li, X., Chen, L., Hou, S., Wu, G., Deng, Z., 2020. A modified soil water content measurement technique using actively heated fiber optic sensor. J. Rock Mech. Geotech. Eng. 12 (3), 608–619.

Wang, J., Zhu, H.H., Mei, G.X., Xiao, T., Liu, Z.Y., 2021. Field study on bearing capacity efficiency of permeable pipe pile in clayey soil: a comparative study. Measurement 186, 110151.

Wang, D.Y., Zhu, H.H., Wang, J., Sun, Y.J., Schenato, L., Pasuto, A., Shi, B., 2023. Characterization of sliding surface deformation and stability evaluation of landslides with fiber–optic strain sensing nerves. Eng. Geol. 314, 107011.

Wu, B., Zhu, H.H., Cao, D.F., Xu, L., Shi, B., 2021. Feasibility study on ice content measurement of frozen soil using actively heated FBG sensors. Cold Reg. Sci. Technol. 189, 103332.

Wu, B., Zhu, H.H., Cao, D.F., Liu, X.F., Liu, T.X., 2023. Fiber optic sensing-based field investigation of thermo-hydraulic behaviors of loess for characterizing land–atmosphere interactions. Eng. Geol. 135, 107019.

Xu, S.H., Li, Z.W., Deng, Y.F., Bian, X., Zhu, H.H., Zhou, F., Feng, Q., 2021. Bearing performance of steel pipe pile in multilayered marine soil using fiber optic technique: a case study. Mar. Georesour. Geotechnol. 40 (12), 1453–1469.

Ye, X., Zhu, H.H., Wang, J., Zhang, Q., Shi, B., Schenato, L., Pasuto, A., 2022. Subsurface multi-physical monitoring of a reservoir landslide with the fiber-optic nerve system. Geophys. Res. Lett. 49 (11), e2022GL098211.

Ying, C., Hu, X., Siddiqua, S., Makeen, G.M.H., Xia, P., Xu, C., Wang, Q., 2021. Model tests for observing the deformation characteristics of micropile boreholes during drilling in a soil-limestone mixture. Bull. Eng. Geol. Environ. 80 (8), 6373–6393.

Zhen, L., Xiong, Y., 2013. Multiscale chemico-thermo-hydro-mechanical modeling of early-stage hydration and shrinkage of cement compounds. J. Mater. Civ. Eng. 25 (9), 1239–1247.

Zheng, X., Shi, B., Zhu, H.H., Zhang, C.C., Wang, X., Sun, M.Y., 2021. Performance monitoring of offshore PHC pipe pile using BOFDA-based distributed fiber optic sensing system. Geomech. Eng. 24, 337–348.

Zhong, R.Y., Guo, R.C., Deng, W., 2018. Optical-fiber-based smart concrete thermal integrity profiling: an example of concrete shaft. Adv. Mater. Sci. Eng., 9290306, 2018.

Zhong, R.Y., Deng, W., 2020. Influence of aggregates in concrete on fiber-optic based thermal integrity profiling analysis of concrete structures. Front. Mater. 7, 227.

Zhu, H.H., Garg, A., Yu, X., Zhou, H.W., 2022. Editorial for Internet of Things (IoT) and artificial intelligence (AI) in geotechnical engineering. J. Rock Mech. Geotech. Eng. 14 (4), 1025e1027.

Zhu, H.H., Wang, J.C., Reddy, N.G., Garg, A., Cao, D.F., Liu, X.F., Shi, B., 2023. Monitoring infiltration of capillary barrier with actively heated fibre Bragg gratings. Environ. Geotech. 10. https://doi.org/10.1680/jenge.21.00130 (in press).

Prof. Honghu Zhu is a Professor at the School of Earth Sciences and Engineering and the Dean of the Institute of Earth Exploration and Sensing, Nanjing University, China. He earned his PhD in Geotechnical Engineering from the Hong Kong Polytechnic University in 2009. His research interests primarily lie in fiber optic monitoring and stability analysis of geoengineering problems, with a special focus on interface behaviors. His research outputs have been applied to many projects, such as landslide monitoring in the Three Gorges Reservoir area, debris flow prevention and control in the Wenchuan earthquake area, and structural health monitoring of the Pearl River Delta water conveyance tunnel. Over the past decade, he has co-authored two books, 12 patents, and published over 100 journal and conference papers. In recognition of his significant contributions to engineering geology and geotechnics, he was awarded the 1st-class Prize of National Scientific & Technological Progress Award of China in 2018 and was awarded funding from the National Science Fund for Distinguished Young Scholars in 2022. He serves as an editorial board member for *Journal of Rock Mechanics and Geotechnical Engineering* (*JRMGE*), *International Journal of Geosynthetics and Ground Engineering*, and *Smart Construction and Sustainable Cities*.